Magnetotail response to prolonged southward IMF B_z intervals: Loading, unloading, and continuous magnetospheric dissipation

E. I. Tanskanen, J.A Slavin, D.H. Fairfield, D.G Sibeck

NASA, Goddard Space Flight Center, Greenbelt, MD, USA

J. Gjerloev

Johns Hopkins University, Applied Physics Laboratory, MD, USA

T. Mukai, A.Ieda

Institute of Space and Astronautical Sciences, Japan

T. Nagai

Tokyo Institute of Technology, Japan

Short title: TAIL CONVECTION MODES

Abstract.

The response of the Earth's magnetotail to prolonged southward interplanetary magnetic field (*IMF*) has been determined for the three Geotail magnetotail seasons from November to April, 1999 – 2002. We examine the total magnetotail pressure $P_{T,tail} = B^2/2\mu_0 + N_i k T_i$, because variations should be similar in this parameter in the lobes and in the plasma sheet. We found 13 events when *IMF* B_z remained southward for 8 hours or longer, and Geotail located within the magnetotail further than 10 R_E downstream. All 13 events were subdivided into separate intervals characterized as (1) loading, if the tail total pressure increased more than 100%; (2) unloading, if the total pressure decreased by more than 50%; and (3) what we term here continuous magnetospheric dissipation (CMD), if the tail total pressure increased by less than 100% and/or decreased less than 50% during the entire mode interval. In total, 37 loading, 37 unloading, and 28 CMD events were found. The plasma sheet magnetic flux transfer rate, $\phi_{Earth} \approx v_x \cdot B_z$, and plasma bulk velocity has been analyzed to determine the steadiness of the plasma sheet convection. Plasma sheet convection was found to be highly disturbed and intense plasma flows (BBFs and FBs) were observed during all convection states. However, the number and amplitude of plasma flows distinguish loading-unloading and continuous dissipation periods from each other. BBFs seem to be more numerous (#135), but weaker (about 500 km/s) during continuous dissipation intervals compared to BBFs existing during unloading mode (#61 and 660 km/s). Finally, it was found that CMD type convection is more likely when the mean southward *IMF* $B_z > -5\ nT$ while loading-unloading is more likely when *IMF* $B_z < -5\ nT$.

1. Introduction

Earth's magnetotail is known to respond to strong solar wind driving in several different ways; southward IMF B_z can lead to isolated magnetotail loading and unloading [*Caan et al.,* 1978], periodic loading and unloading [*Huang et al.,* 2003; *Borovsky et al.,* 1993; *Slavin et al.,* 1992], or steady magnetospheric convection (*SMC*) [*Pytte et al,* 1978; *Sergeev,* 1977; *Sergeev et al,* 1999]. Isolated loading and unloading period exists when the solar wind *IMF* B_z is southward longer than 30 minutes usually in association with substorms [*Akasofu,* 1981]. Southward B_z initiates the dayside reconnection [*Russell and McPherron,* 1973; *Fairfield and Cahill,* 1966]. When *IMF* B_z remains southward for longer than about half an hour, sufficient energy and magnetic flux accumulates within the magnetosphere to power a single substorm [*McPherron et al,* 1973]. Periodic substorms require the *IMF* B_z to be southward for a longer time [*Huang et al.,* 2003] or exhibit several shorter duration southward B_z excursions close to each other [*Borovsky et al.,* 1993; *Slavin et al.,* 1992].

Figure 1.

How the magnetosphere decides which convection mode to adopt is, in principle, the result of the relative flux transfer rates at the two competing sites (see Cartoon in Figure 1). The dayside-to-nightside flux transfer rate (ϕ_d) define how much magnetic flux is transported into the magnetotail per unit time while the nightside-to-dayside flux transfer rate (ϕ_{Earth}) define how much of the available magnetic flux is transported back to the dayside magnetosphere or temporarily stored in the tail lobes. Thus, even if there were a huge amount of magnetic flux flowing into the magnetotail, as is the case during

prolonged southward IMF periods, the magnetic flux directly transported back towards the Earth could exceed, equal, or be less than the rate of inflow to the tail. During the substorm expansion phase the return flow usually exceeds the inflow and previously stored flux is released in addition to the flux which is directly transported from solar wind via tail lobes towards the Earth. At times, nightside reconnection may process all or most of the magnetic flux being added to the tail in a nearly continuous manner. In this case, the magnetotail lobe magnetic field magnitude and the static (thermal and magnetic) pressure at various locations in the magnetotail should stay fairly constant. Under these conditions it has been suggested that plasma sheet convection should be, on average, steady. In fact, some examples of what is termed steady magnetospheric convection have been reported [*Sergeev et al.* 1977; *Sergeev, V. A. and Lennartsson, W.* 1988; *Yahnin et al.* 1994; *Sergeev et al.* 1996A; *Sergeev et al.* 1996B; *Shukhtina et al.* 2004], and invoked to explain activity observed on the ground [*O'Brien et al.* 2002]. However, the characteristics of plasma sheet convection during loading-unloading intervals are poorly understood, while those of plasma sheet convection during periods of steady tail pressure intervals remain largely unstudied. We term the latter intervals, with relatively constant tail total pressure, as 'continuous magnetospheric dissipation' (CMD) intervals (Figure 1).

Theoretical issues surrounding the possibility of steady adiabatic convection have been presented by *Erickson and Wolf* [1980]. They suggested that "steady adiabatic convection probably cannot occur through a closed-magnetic-field-line region that extends into a long magnetotail". The argument is that if steady adiabatic convection

were to exist then there would be a pressure-balance crisis due to the large difference in volume between magnetic flux tubes in the inner and outer plasma sheet. If no particles are lost as flux tubes convect Earthward, then extremely high plasma β (ratio between thermal and magnetic pressure) conditions would develop in the inner plasma sheet. These high plasma thermal pressures in the inner plasma sheet would, in turn, depress the magnetic field intensity and oppose continued Earthward convection. This pressure balance crisis is, in fact, not observed at least on the basis of the magnetic field profiles in the inner tail [see *Spence et al.,* 1987]. The pressure balance crisis can be avoided through particle loss due to precipitation into the the upper atmosphere, enhanced drift to the flanks of the tail, plasmoid ejection down the tail, or by plasma sheet convection that proceeds only in an episodic manner as is seen in bursty bulk flows [*Baumjohann et al.* 1990; *Angelopoulos et al.* 1992],.

Many studies (e.g. about BBF's) have focused on the plasma sheet during substorms, but few SMC's are reported. *Sergeev* [1977] and *Pytte et al.* [1978] first identified SMCs on the basis of auroral zone magnetic measurements. SMCs are thought to occur when there is "enhanced energy input from the solar wind into the magnetosphere over a time period of several substorm time constants" [*Sergeev et al.,* 1996A]. However, it is not known whether SMCs occur every time when the solar wind feeds the magnetosphere over several hours in a steady manner, how steady plasma sheet convection really is during SMCs, and whether steady convection periods lasts over the entire period of enhanced input or whether loading-unloading periods (i.e. substorms) interrupt SMCs at times. Plasma sheet convection itself has been extremely

difficult to track due to the rarity of continuous plasma sheet measurements over such extended intervals. As far as we know only a few papers have directly examined plasma sheet convection during SMCs [*Petrukovich et al.,* 1999; *Yermolaev et al.,* 1999; *Sergeev et al.,* 1990].

The most frequently used operational definition for SMC identification in based on the ground-based electrojet index AE. *Sergeev* [1996A] identified events on the basis of enhanced AE index without any clear substorm signatures. Recently, *O'Brien et al.* [2002] presented a large statistical survey of SMCs based on AE-level and AL stability. They found about 350 SMCs (non-substorm periods) in 18 months while typically such an interval would include about 1500-2000 substorms [*Borovsky et al.,* 1993; *Kamide et al.,* 1982].

In this paper, we examine loading, unloading, and continuous magnetospheric dissipation intervals during prolonged southward $IMF\ B_z$ intervals. We chose to use total magnetotail pressure as an operational criterion to distinguish different convection modes. That is because the total pressure is expected to be relatively insensitive to the spacecraft location due to the pressure balance condition at any given X location at the magnetotail. Pressure does vary along the tail in X direction, but the gradients are small (i.e. factor of 2 every 10 R_e). Continuous magnetospheric dissipation occur when the tail total pressure exhibits no strong loading and unloading signatures. The outstanding question that this paper attempts to answer is how the tail responds to extended intervals of $IMF\ B_z < 0$? We will show that the magnetotail response may be described as occurring in three modes: loading, unloading and continuous

magnetospheric dissipation. In all modes plasma sheet convection was found to be dominated by bursty bulk flows and no intervals of steady magnetospheric convection were observed. Finally, the possible external causes of each mode are investigated.

2. Prolonged southward *IMF* B_z

ACE upstream magnetometer data in 12 second resolution was used to search for intervals when the *IMF* B_z was continuously southward for periods longer than two hours. ACE data was convection shifted to the magnetopause at 10_{R_e} by $\Delta t = \Delta X/v$, where v is the average velocity during the mode interval. The three latest Geotail seasons in the magnetotail, November through April from 1999 to 2002, were used. A total of 382 events were found. Figure 2 shows a histogram of all *IMF* B_z southward intervals longer than two hours. It shows that the likelihood of encountering a southward interval decreases exponentially with interval length. The longest southward event in our data set was about 31 hours. Intervals of prolonged southward *IMF* orientation are extremely common in solar wind; almost every day ACE observed at least one southward interval longer than two hours and at times even four 2 hour intervals were observed on the same day.

Figure 2.

For the purpose of examining the magnetotail response to prolonged southward *IMF* B_z we have selected intervals when the B_z was negative for longer than eight hours, which is more than two times the duration of a typical substorm [*Akasofu et al.* 1981; *Tanskanen et al.* 2002]. We found 52 such events within our one and half year data base satisfying this requirement (Appendix I).

3. Magnetotail convection modes

Geotail magnetic field and plasma data were used to determine the response of the magnetotail to *IMF* B_z intervals lasting longer than 8 hours. Geotail was required to be in the tail further than 10 R_E from the Earth, and not too far side from Sun-Earth line (GSM y,z) such that solar wind flow would have been observed. This condition was met for 13 events out of the 52 *IMF* B_z^- intervals lasting longer than 8 hours. The total tail pressure was computed for the 13 events as the sum of the thermal and magnetic pressures

$$p_{T,tail} = N_{i,tail}\, k_B\, T_{i,tail} + \frac{B_{tail}^2}{2\mu_0}, \tag{1}$$

where $N_{i,tail}$ is the ion number density, $T_{i,tail}$ the ion temperature, B_{tail} the magnitude of tail magnetic field, k_B Boltzmann's constant, μ_0 the magnetic permeability of free space, m_p the mass of proton, and v the plasma bulk velocity.

As discussed earlier, we use the variation in total tail pressure to identify different convection modes. We identified loading intervals as those with total pressure increases greater than 100%, and unloading intervals as those with total pressure decreases more than 50%. All other intervals with the total pressure increases less than 100% and total pressure decreases less than 50% were labelled 'continuous magnetospheric dissipation' (CMD), which are also our candidates to be steady magnetospheric convection events. The minimum mode duration was arbitrarily set to 1/8 of the substorm convection cycle or 30 minutes.

	Mode definition	Operational def.
Loading	$\int \phi_d dt > \int \phi_{Earth} dt$	$p_2/p_1 > 2$
Unloading	$\int \phi_d \, dt < \int \phi_{Earth} \, dt$	$p_2/p_1 < 0.5$
CMD	$\int \phi_d \, dt \approx \int \phi_{Earth} \, dt$	$0.5 > p_2/p_1 > 2$

Table 1. Definitions and operational definitions of convection modes. Used symbols are dayside-to-nightside flux transfer rate (ϕ_d), nightside-to-dayside flux transfer rate (ϕ_{Earth}), tail total pressure in the beginning of the mode interval (p_1), and tail total pressure in the end of the mode interval (p_2).

Earlier mentioned 13 prolonged southward *IMF* B_z intervals can be divided into 102 events corresponding to these three convection modes. Figures 3a, 5a, and 6a display Geotail plasma ion beta ($\beta_{i,tail}$), the z-component of the tail magnetic field ($B_{z,tail}$), the tail pressures (total, magnetic and thermal), and the x-component of the tail flow velocity ($v_{x,tail}$) for the events on April 15-16, 2000; February 13-14, 2001; and December 29, 2000. The black curve in third panel indicates the total pressure ($P_{T,tail}$),

the blue curve the magnetic pressure ($P_{magn,tail}$), and green curve thermal pressure ($P_{th,tail}$). Velocities in the fourth panel are color-coded such that Earthward velocities in the plasma sheet are marked by blue, tailward velocities by red, and velocities measured when the Geotail was in the lobe or plasma sheet boundary layer (PSBL) are color-coded light red and light blue (only in Figures 5a, and 6a). The ratio of the plasma ion pressure to the magnetic pressure

$$\beta_{i,tail} = \frac{N_{i,tail}\, k_B\, T_{i,tail}}{B_{tail}^2/2\mu_0}, \tag{2}$$

is used to identify the plasma regimes the Geotail is located. When $\beta_{i,tail} > 0.1$ Geotail is in the plasma sheet, when $\beta_{i,tail}$ is less than or equal to 0.1 the Geotail is in the tail lobes or the plasma sheet boundary layers [*Slavin et al.,* 2003; *Baumjohann et al.,* 1990]. Below the panels we show Geotail location (x, y, and z) in GSM coordinates.

Solar wind conditions during the different tail responses were analyzed using three parameters: solar wind speed ($v_{x,sw}$), ion density (N_i), and dynamic pressure (P_{dyn}) (Figures 3c, 5c, and 6c). The state of the entire magnetosphere is monitored by two well-known indices: approximate ring current index, Dst, and westward electrojet index (Figures 3d, 5d, and 6d). Instead of standard westward electrojet index we use extended westward electrojet index, AL_n specifically prepared to this study, where n is the number of stations included in to the envelope computation. For our example events we included data for about 25 evenly distributed observatories around the globe. The standard AL index normally only includes magnetic observations for less than 10 stations. The purpose of using extended AL is to obtain a magnetometer grid dense

enough to determine whether auroral zone activity is enhanced, but steady without the sharp decreases interpreted as a substorm onsets. The Dst index was used to assess 'the storminess' of the magnetosphere. About two thirds (8) of the southward periods produced storms while one third (5) of the southward intervals corresponded to non-storm times with Dst greater than -40 nT. All eight storm-time southward periods occurred at the storm initial phase, before the peak of the storm maximum intensity. It was interesting to note that more than half of the continuous dissipation events occurred during storm times.

3.1. Loading mode: April 15-16, 2000

Figure 3.

Figure 3 shows an example of an extended loading mode. The loading period starts around 2300 UT at April 15-16, 2000 when Geotail was located in the central plasma sheet, CPS, ($\beta_i > 1$). Using our criteria, the loading mode continues more than 6 hours until 0520 UT when the *IMF* B_z turns northward. This extended loading follows 2-hour period with reasonably steady tail total pressure when the average total pressure $P_{T,tail}$ is 0.15 nPa and standard deviation for pressure is 0.03 nPa. During the period of steady total pressure, Geotail observes multiple Earthward and tailward bursty bulk flows in the plasma sheet. The tail velocity calms down, being weak after 0100 UT and almost zero between 0200 and 0300 UT, during tail loading (Figure 4). We interpreted this as evidence indicating that the energy being added to the tail in the form of lobe magnetic flux is only very weakly dissipated with little flow and no BBFs. Not displayed is the POLAR VIS imaging (J. Sigwarth private communication, 2004) that showed

an increasing polar cap size as the loading proceded (images available on 25th from 21:00 to 23:00 UT and on 26th from 01:00 to 02:00 UT). During the extended loading mode the total pressure increases from 0.25 nPa up to 1 nPa, average total pressure $\mu(P_{T,tail})$ being 0.5 nPa and standard deviation $\sigma(P_{T,tail})$ 0.23 nPa. The increase of the tail magnetic pressure may be partly because the spacecraft moves towards the Earth and starts to see the dipole field. However, the increase in total pressure can not be only spatial because for this event the magnetic pressure does not dominate in the total pressure computation.

Figure 4.

Geotail travels from -20R_E to -11R_E in about eight and half hours (Figure 3b). The spacecraft stays very close to the equatorial plane, $z_{GSM} \approx 0$, and it remains deep in the central plasma sheet during entire southward *IMF* B_z period. This can be interpreted as evidence either for a very stable magnetotail and/or a very thick plasma sheet. The solar wind velocity (Figure 3c first panel) was also extremely stable, with standard deviation $\sigma(v_{x,sw}) = 3.7\ km/s$, and low, with average $\mu(v_{x,sw}) = -320\ km/s$, during the extended loading mode. Proton density and dynamic pressure showed slowly increasing trends; proton density increasing from 10 to 20 particles/cm^2 and dynamic pressure from 2 to 4 nPa in six hours. These increasing trends on solar wind density and dynamic pressure may be part of a reason to get the extended tail loading.

3.2. Unloading: February 13-14, 2001

Figure 5.

February 13-14, 2001 provides an example of two loading-unloading periods followed by one more loading and a continuous dissipation period (Figure 5). Two unloading

periods starts at 1840 and 2130 UT and ends at 1915 and 2230 UT, respectively. The first loading period lasts about 30 minutes and the second about an hour, which are both known to be typical unloading mode durations [e.g. *Slavin et al.,* 2003; *Caan et al.,* 1973]. Both unloadings give nice substorm signatures; the westward electrojet enhancement and a sharp decrease during the onset (Figure 5d). The tail total pressure varies between 0.2 and 0.6 nPa being highest at the beginning and lowest at the end of the two unloading phases. That is at the same level, but slightly less variable than during the previous example. Geotail travels from x_{GSM} = -17 to -23 R_E and according to plasma ion beta it stays mostly in the plasma sheet. Only during two unloading periods when the plasma sheet probably becomes quite thin(plasma sheet thinning during unloading mode is suggested e.g. by MHD simulation results of [*Lee et al.* 1985]) did Geotail find itself in the tail lobes. Velocities in the plasma sheet reach 1600 km/s during loading and steady pressure intervals. Geotail velocity measurements do not give much information about plasma sheet velocities during the unloading mode, because of lack of plasma sheet observations caused by the plasma sheet thinning. Nevertheless, the Geotail observes plasma bursts in the tail lobes, plasma sheet boundary layers and most probably also in the plasma sheet. In addition, the extended electrojet index (Figure 5d) shows strong substorm activity and the tail unloading phases occurred during an initial phase of a small storm with the Dst minimum -50 nT.

At the beginning of the southward period *IMF* B_z decreases to -10 nT, from where it slightly increases close to zero at the end of the second unloading period. Average interplanetary B_z is about -9.0 and -3.0 nT during unloading, -6.6, -6.6, and -2.4 nT

during loading and about -3.1 nT during steady pressure intervals. Solar wind density and dynamic pressure remained extremely constant (around 5 particles/cm^3 and 2 nPa) and solar wind velocity decreased slightly for continuous dissipation period being around -530 km/s before the mode and about -510 km/s during the mode.

3.3. Continuous magnetospheric dissipation (CMD): December 29, 2000

Figure 6.

A seven hours long continuous magnetospheric dissipation interval was identified on December 29, 2000 (Figure 6). The interval started at 0500 UT when Geotail was located 20 R_E at the nightside (GSM -20, -13, -2 R_E); the spacecraft spends the entire period deep in the plasma sheet. A steady total pressure period followed another steady period and a quick unloading mode, which dropped the tail total pressure from 0.25 to below 0.1 nPa. The AL_{26} (Figure 6d) shows enhanced, but fairly constant activity during the continuous dissipation modes and a sharp decrease at the time on tail lobe unloading. The substorm is strong with maximum amplitude more than 800 nT, but very localized; only two stations, Baker Lake and Fort Churchill, show AL_{26} below -300 nT. The standard AL index would have missed the sharp decrease entirely and the maximum amplitude of the substorm would have been only 200 nT. During the second CMD interval the tail total pressure is extremely low being under 0.1 nPa during entire mode.

Plasma flow is mainly Earthward reaching its peak value -1020 km/s at the very beginning of the continuous dissipation interval and being highly variable throughout the mode. We count 28 plasma bursts from $|v_{x,tail}|$ using a lower limit for BBF identification

of 200 km/s. We define BBF durations in such way that the BBF starts when $|v_{x,tail}|$ first reach 20 km/s and BBF ends when $|v_{x,tail}|$ returns back to 20 km/s. We find an average BBF duration of 8 minutes in contrast with the 10 – 20 minutes mean duration found in the surveys by *Baumjohann et al.* [1990], *Angelopoulos et al.* [1992] and *Nagai et al.* [1998]. Our result for BBF duration agrees nicely with the result of earlier studies when it is taken into account that our amplitude limit to identify BBFs is lower compared to the earlier studies.

4. How steady are the magnetotail and plasma sheet during different convection modes?

4.1. Magnetotail stability

Figure 7.

Total pressure, plasma bulk velocity ($|v_{x,tail}|$) and electric field ($E_{y,tail}$) have been used to examine the variability of the Earth's magnetotail during continuous magnetospheric dissipation intervals. The tail conditions during CMDs are compared to the conditions during the loading and unloading phases. A total of 102 mode intervals were analyzed, of which 37 were loading modes (black circles in Figure 7a), 37 unloading modes (white circles), and 28 met our criteria for CMD (stars). Tail total pressures at the beginning of the mode intervals are plotted against the total pressures at the end of the modes to show the definitions which have been used for different convection modes. Two black lines (100 % increase and 50% decrease) separate the three convection modes from each others. There seems to be a continuum of events from one mode

to another one, and the selection criteria presented in the second paragraph of the Section 3 could have been different e.g. such that also weaker loadings/unloadings or loadings/unloadings in shorter time scales than 30 minutes would have been included. Average mode duration for loading was 95 minutes, for unloading 48 minutes, and for continuous magnetospheric dissipation 137 minutes. In addition to these basic modes we defined extended modes when their duration exceeded three hours. We found 4 extended CMD intervals (of which one is described in Section 3.1.) and 3 extended loading intervals (of which one is described in Section 3.3), but no extended unloading intervals. It is clear from our analysis that unloading mode is the most rapid, while CMDs are the longest. The CMD events can last from tens of minutes to several hours.

In Figure 7b we show average tail total pressure versus total pressure standard deviation for loading, unloading and CMD coded similarly as earlier. The average total pressures are quite similar for all modes, varying between 0.05 and 0.9 nPa for each mode. But, the standard deviation is clearly much lower for continuous dissipation mode than for the two other modes giving values between 0.005 and 0.18 nPa for CMD mode and between 0.025 and 0.32 nPa for loading and unloading modes. **Figure 8.**

Tail total pressure variability (coefficient of variation, CV) is measured by the ratio between the standard deviation and the average total pressure

$$CV(P_T) = \frac{\sigma(P_T)}{\mu(P_T)} \cdot 100\%. \quad (3)$$

For an example extended loading mode, April 15-16, 2000 at 2300 - 0520 UT, the tail total pressure steadiness parameter was 46%, while it was 38% and 35% for two

unloading periods on February 13-14, 2001, and 16% for the extended CMD, December 29, 2000. The coefficient of variation is computed for all the 102 mode intervals from where we conclude that 20% variation can be kept as a border line between CMD and two other modes. As seen in Figure 7b almost all CMD intervals locates below the 20%-line and main part of the other modes are above the line. In Figure 8 we show histograms of $CV(P_T)$ separately for loading-unloading and continuous dissipation modes. Histogram for CMD mode peaks at 15% and histogram for loading and unloading modes peak at 30%. According to the total pressure the CMD intervals really are steadier than the two other intervals, which is not too surprising because of our definitions.

Two other magnetotail parameters, velocity, and electric field, were highly disturbed compared to the steadiness of the tail total pressure. The total tail velocity $v_{x,tail}$ showed high speed plasma flows during each of the three modes (Figure 9). Plasma bulk velocity varied between -2318 (tailward) and 2110 km/s being slightly more often Earthward. Steadiness of velocity described by average coefficient of variation was around 90% for unloading phase and slightly below 80% for two other modes. Electric field, $E_{y,tail} = v_x \cdot B_z$ showed even more variability than a plasma bulk speed. Tail electric field was variable and spiky for all modes giving extremely low steadiness values; average standard deviation was almost 2 sigmas (200%) from the mean electric fields for all three mode intervals. From Geotail measurements at the Earth's magnetotail we conclude that entire tail is highly disturbed during prolonged southward periods independent of the convection mode.

4.2. Plasma sheet activity

Two most important parameters characterizing the plasma sheet (PS) convection are plasma sheet velocity, $v_{x,PS}$, and magnetic flux transfer rate

$$\phi_n = v_{x,PS} \cdot B_{z,PS} \cdot L, \tag{4}$$

where L is the length of the x-line at the tail. A net transport of southward magnetic flux out of the tail corresponds to a positive flux transfer rate. We used velocity and flux transfer rate to examine the plasma sheet convection during loading, unloading and CMD intervals. The analysis was repeated with plasma sheet criteria $\beta_i > 0.1$, $\beta_i > 0.3$ and $\beta_i > 0.5$, which did not critically affect the results presented here.

	Loading	Unloading	CMD
BBF #	83	61	135
T [h]	47	19	50
Δt	7min 17s	6min	7 min 8 s
f [1/min]	1/40	1/19	1/22
A [km/s]	523	663	496
$(\# \cdot \Delta t)[h]$	10	6	16
$(\# \cdot \Delta t)/T[\%]$	21	32	32
Earth and tailward			
$(\# \cdot \Delta t)[h]$	18	15	22
$(\# \cdot \Delta t)/T[\%]$	37	78	45

Table 2. Earthward plasma sheet bursty bulk flow, BBF, characteristics during loading, unloading and continuous magnetospheric dissipation (CMD). Parameters from top to bottom are number of BBF (#), total duration Geotail spent in plasma sheet (T), average BBF duration (Δt), BBF frequency, BBF maximum amplitude (A), and time in hours $(\# \cdot \Delta t)$ and in percents $(\# \cdot \Delta t)/T$ that there was BBF activity in the plasma sheet. Two last lines are the time in hours $(\# \cdot \Delta t)[h])$ and in percents $(\# \cdot \Delta t)[h])$ when

both tailward and Earthward velocity bursts are taken into account.

Two type of plasma sheet flows, bursty bulk flows (BBFs) and flow bursts (FBs) are examined. BBFs are defined to be high velocity plasma bursts in plasma sheet in time scales of 10 - 20 minutes and FBs are high velocity plasma bursts in time scales of a few minutes [*Angelopoulos et al.,* 1992; *Baumjohann et al.,* 1990]. In this study the 200 km/s limit for velocity is used to define both BBFs and FBs. The duration of BBFs is defined from 20-to-20 km/s and the duration of FB is taken from 200-to-200 km/s. In total, 294 Earthward traveling BBFs are observed of which about half were seen during CMDs (Table 2). Average Earthward BBF duration based on this data set is slightly over 7 minutes for loading and CMD intervals, and about a minute less for unloading mode BBFs. When both Earthward and tailward BBFs are taken into account the plasma sheet was found to be active half of the time during CMDs, about 80% of the time during unloadings, and one third of the time during loading phase. The characteristic time scale for Earthward flow bursts was found to be 1 to 2 minutes (Table 3). Largest difference between Earthward flowing FBs occurring during CMDs and unloading modes was that the average peak amplitude was 403 km/s for CMD and 523 km/s for unloading mode FBs. Surprisingly, intense flow bursts up to 1834 km/s also occurred during loading, which we interpreted that plasma sheet is also highly active during loading. If stricter β_i-criteria were used, then the maximum loading mode FP intensities would have been 1834 km/s (for $\beta_i > 0.3$) and 1560 km/s (for $\beta_i > 0.5$).

	Loading	Unloading	CMD
FB #	193	113	274
T [h]	47	19	50
Δt	1min 17s	1min 41s	1 min 25s
f [1/min]	1/15	1/10	1/11
A [km/s]	420	523	403

Table 3. Earthward plasma sheet flow burst, FB, characteristics during loading, unloading and continuous magnetospheric dissipation (CMD). Parameters from top to bottom are number of FB (#), total duration the Geotail spent in plasma sheet (T), average FB duration (Δt), FB frequency, and average FB amplitude (A).

In Figure 9 we show histograms of entire velocity data separately for three convection modes. Earthward and tailward flows occur during all modes. The plasma sheet flow was mostly Earthward for CMDs (70% of the time) and for loading periods (64% of the time), and half Earthward and half tailward for the unloading intervals. That can be interpreted as an indication that the spacecraft spent most of the time Earthward of the near-Earth neutral line (NENL) during CMD and loading periods, but was close to the NENL during unloading intervals. Thus, either NENL was located on

average more distant to Earth during CMD than during unloading mode, or the Geotail spent more time closer to the Earth for CMDs.

Figure 9.

The tail-to-Earth magnetic flux transfer rate per unit length ϕ_{Earth}/L was computed separately for all convection modes (Table 4). The average transfer rate for loading, unloading and CMD was, correspondingly, 0.28, 0.19 and 0.41 mWb/m$\cdot$ s showing that the flux transfer rate at Geotail as well as the velocity were most strongly Earthward for CMDs. The average flux transferred Earthward through the plasma sheet, $\mu(\phi_{Earth}/\mathrm{L})$, was largest during unloading mode (0.80 mWb/m$\cdot s$) as would be expected. The average flux transferred during CMDs was only slightly smaller, 0.77 mWb/m$\cdot$ s, while that during loading modes was somewhat smaller, 0.62 mWb/m$\cdot$ s. The net flux transfer during all three convection modes is Earthward, which is presented in first line of Table 4. Table 4 also shows the standard deviation and coefficient of variation for absolute transfer rates per unit length, which clearly shows that the flux transfer is far from being steady for each type of convection modes.

	Loading	Unloading	CMD
$\mu(\phi_n/\mathrm{L})$	0.28	0.19	0.41
$\mu(\phi_{Earth}/\mathrm{L})$	0.62	0.80	0.77
$\mu(\phi_{sw}/L)$	-0.28	-0.54	-0.33
$\sigma(\phi_{Earth}/L)$	1.2	1.3	1.2
$\sigma(\phi_{sw}/L)$	0.4	0.9	0.6
$\mathrm{CV}(\phi_{Earth}/L)$	188%	159%	176%
$\mathrm{CV}(\phi_{sw}/L)$	155%	176%	190%

Table 4. Average (μ), standard deviation (σ) and coefficient of variation (CV) for plasma sheet magnetic flux transfer rate per unit length during loading, unloading and continuous magnetospheric dissipation intervals. Earthward flux (ϕ_{Earth}/L) and flux back to solar wind (ϕ_{sw}/L) are shown separately, and all units are $mWb/m \cdot s$ if not otherwise stated.

To summarize, the Geotail magnetotail and plasma sheet observations during continuous magnetospheric dissipation show clearly that they are far from being intervals of steady plasma sheet convection. Particularly, the plasma sheet velocity was found to be mostly fast during CMDs. In addition, the plasma sheet flux transfer rate characterizing the plasma sheet convection was mostly high and very disturbed. Only

at times the convection was slow with the convection velocity less than 100 km/s, which happened when the tail total pressure was slowly increasing representing the extended magnetotail loading.

5. Solar wind conditions leading to different tail responses

Figure 10.

Upstream solar wind conditions, $IMF\ B_z$, total ($P_{T,sw}$) pressure, plasma convection speed ($v_{x,sw}$) and electric field ($E_{y,sw}$), have been examined to identify the possible solar wind precursors for loading, unloading and continuous magnetospheric dissipation. Different modes in the February 2001 example (Section 3.2) are fairly typical in terms of solar wind parameters; $IMF\ B_z$ gives slightly negative values, around -3 nT, for continuous dissipation mode and more negative values, around -5 nT, for two other modes. Statistical study of 102 modes gives histograms for $IMF\ B_{z,sw}$ seen in Figure 10. Panels in left (10) we show histograms of average $IMF\ B_{z,sw}$ ($\mu(IMF\ B_{z,sw})$) for three modes. Average B_z for continuous dissipation peaks at higher values compared to two other modes; the mean $IMF\ B_{z,sw}$ is -4.8 nT for CMD mode and about -6.6 nT for the loading and unloading modes. Histograms of minimum southward magnetic field during the entire mode interval ($\min(IMF\ B_{z,sw})$) are similarly plotted separately for three modes (panels in middle in Figure 10b). The mean of the minimums for the unloading modes is around -9 nT, for the loading modes -8 nT, and for the CMD modes around -7 nT. Panels in left (10c) give a standard deviation for southward magnetic field. Standard deviation seems to be almost equal, around 1 nT, for all modes. Extended loading and extended CMD modes locates in the right-hand-side of the histograms (i.e.

less negative $IMF\ B_z$) implying that magnetosphere needs to be driven smoothly to get modes lasting longer than three hours.

Solar wind total pressure is computed as the sum of thermal ($p_{th,sw}$), magnetic ($p_{magn,sw}$) and dynamic pressures ($p_{dyn,sw}$)

$$P_{T,sw} = N_{i,sw}\, k\, T_{i,sw} + \frac{B_{sw}^2}{2\mu_0} + N_{i,sw} m_p\ v^2, \tag{5}$$

where parameters are proton number density $N_{i,sw}$, Boltzmann constant k, proton temperature $T_{i,sw}$, magnetic field magnitude B_{sw}, proton mass m_p and v plasma bulk velocity. Average and steadiness of solar wind total pressure were quite similar for all modes; average total pressure was 2.4 nPa for loading and unloading modes, and 2.7 nPa for CMD mode, and coefficient of variation about 18% for all modes. **Figure 11.**

By comparing histograms in Figure 8a and in Figure 11 it can be seen that the disturbance level (CV) of solar wind total pressure is very similar, on average, than the disturbance level in the tail total pressure during continuous magnetospheric dissipation. For substorm (loading and unloading) intervals the tail pressure disturbances are about twice as big, on average, compared to solar wind pressure disturbances. For analyzing whether short time scale pressure variations at magnetotail can be caused by solar wind pressure variations we computed correlation between $p_{T,tail}$ and $p_{T,sw}$. The linear correlation coefficient for loading and unloading intervals was 0.05, and for continuous magnetospheric dissipation intervals -0.02. Thus, it seems evident that short time scale variations in magnetotail total pressure are not a linear consequence of solar wind

pressure variations.

Solar wind profiles or average solar wind velocities did not show clear differences between different modes (not shown here). Similarly point-by-point correlation between tail and solar wind electric fields (E_y) did show very low correlation for all modes. However, we did not produce a detailed analysis about E_y trends and disturbance levels. As a summary of solar wind precursors, we conclude that the only solar wind parameter that clearly distinguishes different tail modes from each others is the level of $IMF\ B_z$. All other parameters, uncorrected and flaring angle corrected solar wind pressures, electric field and average solar wind speed and trends, did not show clear or any differences between loading, unloading and continuous dissipation modes.

6. Discussion

The purpose of this paper was to examine the magnetotail responses to prolonged $IMF\ B_z$ intervals. We found that periods of prolonged solar wind driving, lasting more than two hours, occur almost every day. The total magnetotail pressure was selected to identify different responses, because pressure is expected to be insensitive to whether or not the spacecraft is in the plasma sheet [e.g. *Fairfield et al.,* 1981]. Three different tail responses were identified: (1) Magnetic flux loading to the tail lobes, (2) magnetic flux unloading, and (3) continuous magnetospheric dissipation (CMD), where the dayside and nightside flux transfer rates balance each other in a quasi-continuous manner. CMDs differ from SMC intervals such that during continuous dissipation the plasma sheet is highly active while during steady convection the plasma sheet and the entire

magnetotail should be fairly stable.

Continuous magnetospheric dissipation was found to be almost as common as the loading and unloading modes associated with substorms. In total, we found 28 CMDs, 37 loading, and 37 unloading periods. Unloading intervals are clearly the shortest lasting on average 45 minutes. This result agree very well with 40 min in *Caan et al.* [1978]. The loading intervals typically last about 90 minutes or about twice the unloading duration, while the continuous dissipation last about three times as long or about 137 minutes.

For the purpose of the mode identification we use "200% criteria". That counts the loadings when the tail static pressure increase is 100%. Similarly only intervals with more than 50% decrease are count as unloading modes. By using these criteria we select only strong loading and unloading periods. Weaker loadings and unloadings would have been included to the study if smaller pressure changes will be counted. However, in this paper we examined tail response to the strong solar wind driving, which means long periods of negative $IMF\ B_z$, and now the "200% criteria for mode identification is justified.

Distribution of plasma sheet bulk speed, and electric field were examined for all three convection states. Average steadiness was assessed using a coefficient of variation equal to the ratio of the standard deviation to the mean. In this manner, the coefficient of variation was 90% for bulk speed, and as large as 200% for electric field. By comparison, average CV for tail static pressure was only 7% for continuous magnetospheric dissipation periods, and 3% for loading and unloading intervals. In this

study we examined the tail parameters using 12 s resolution data. We speculate that the apparent steadiness of plasma sheet convection reported for some previously published case studies [e.g. *Sergeev et al.,* 1996A] may be due to the use of lower resolution or averaging over longer periods. The large differences in the apparent steadiness of tail flows depending upon which data resolution is used suggest that the magnetotail has a characteristic time scales to transport the plasma in a steady manner, which is rather several minutes than seconds. But, on short time scales the tail convection pattern looks highly structured and possibly localized. However, using one-point measurements it is extremely difficult to tell whether observed changes are temporal or spatial.

Plasma sheet convection can be characterized by plasma bulk velocity, and magnetic flux transfer rate. In total, Geotail spend 116 hours in the plasma sheet. Bursty bulk flows and flow bursts were observed during all convection states, but more often during unloading and continuous dissipation periods. BBFs were observed about 80% of the time during unloading, about half of the time during CMD, but only one third of the time during loading intervals. Average BBF intensity was around 660 km/s during unloadings and around 500 km/s during CMDs. Flow bursts forming BBFs lasts typically from 1 to 2 minutes. The flow burst duration agrees well with the results of previous papers [e.g. *Angelopoulos et al.,* 1992, 1993]

The relative importance of a different convection states as a flux carrier was examined by computing Earthward flux transfer rater per unit length $|\phi_{Earth}/L|$. Relatively largest amount of magnetic flux, 0.80 $mWb/m \cdot s$, was carried during unloading, as could be expected, but almost equal amount during CMDs, 0.77 $mWb/m \cdot s$. During

loading mode the flux transfer rate was smaller (0.62 $mWb/m \cdot s$) than during other two convection modes. However, since the rate of flux supply from dayside reconnection is greater for unloading and loading (ϕ_d = 3.0 mWb/m $\cdot$ s, on average) compared to continuous dissipation intervals (ϕ_d = 2.1 mWb/m $\cdot$ s, on average), the total rate of nightside reconnection ϕ_{Earth} needs to be greater for unloading as opposed to continuous dissipation. And since ϕ_{Earth}/L is the same for both unloading and CMD intervals we may conclude that the length of the x-line in the tail, L, for unloading and loading modes is greater than L for continuous dissipation. The steadiness (CV) of the tail-to-Earth flux transfer rates were close to 200% for all modes interpreting that the flux was carried through the plasma sheet towards the Earth in a bursty manner. Thus, when the plasma sheet stability is used as a criteria for steady magnetospheric convection, we did not found such periods.

Solar wind conditions leading to substorms have often been studied. Southward $IMF\ B_z$ opens the magnetosphere letting the solar wind plasma to be mixed with magnetospheric plasma [e.g. *Pachmann et al.,* 1979; *Aubry,* 1971]. Prolonged strongly negative $IMF\ B_z$ causes long duration effects i.e. storms, whereas weak or brief intervals of negative $IMF\ B_z$ cause shorter duration effects. e.g. substorms. It has been, however, largely unknown how the $IMF\ B_z$ behaves before the intervals without loading and unloading signatures (including both CMDs and SMCs). *Sergeev et al.* [1996A] concluded that negative $IMF\ B_z$ plays an important role for SMCs, while *O'Brien et al.* [2002] recently suggested that the $IMF\ B_z$ is weakly negative when the SMC occur. Consistent with *O'Brien et al.* [2002], we found the average $IMF\ B_z$

preceding CMDs to be -5 nT, while B_z is about -7 nT during the loading and unloading modes.

The steadiness of the $IMF\ B_z$ was not found to be an important precursor for continuous magnetospheric dissipation. The result agrees well with results of *O'Brien et al.* [2002], who concluded that the steadiness of the $IMF\ B_z$ has only a slight importance. However, we did not found any SMCs when the steadiness of plasma sheet convection was part of the criteria. Our results suggest that the best way to predict the mode of the magnetotail convection during enhanced solar wind driving is to monitor the level and trend of $IMF\ B_z$ over a longer time period.

7. Summary

The magnetosphere was observed to have three basic ways to respond to prolonged negative *IMF* B_z: loading, unloading and continuous magnetospheric dissipation (CMD). CMDs are for the first time identified in this paper. They are defined as a relatively constant magnetotail total pressure intervals without large increases (100%) or large decreases (50%). CMDs, as well as loading and unloading periods, are a common phenomena in the Earth's magnetosphere; a total of 28 continuous magnetospheric dissipation intervals were found during three Geotail tail seasons (1999-2002). Only slightly more loading (37) and unloading (37) intervals were found during the same time period. In this statistical survey the plasma sheet was observed to be highly disturbed and very bursty during all convection modes. When Geotail spacecraft was in the plasma sheet ($\beta_i > 0.1$) it observed bursty bulk flows about half of the time (45%)

during CMDs and more than 2/3 of the time (78%) during unloadings, and 1/3 of the time during loading (37%) phases. Continuous magnetospheric dissipation was observed to occur during both stormy and non-stormy periods. More than half of the CMDs occurred during stormy magnetosphere when the Dst is used as a storminess indicator.

Next we summarize the rest of the main results of this paper:

(1) Number and amplitude of plasma flow events (includes both BBFs and FBs) distinguish loading-unloading and continuous dissipation intervals from each other. Plasma flows seem to continue intermittently during continuous dissipation intervals (see Figure 6a lowest panel) while flows decrease dramatically when loading mode progresses (as seen in Figure 3a lowest panel). For entire statistics we conclude that in total 135 BBFs were observed during CMDs while 61 BBFs were seen during unloading phases. Maximum amplitude of plasma flows was larger during unloading periods (BBF 663 km/s, FB 523 km/s) compared to continuous magnetospheric dissipation intervals (BBF 496 km/s, FB 403 km/s).

(2) The average magnetic flux transfer rate per unit length, ϕ_{Earth}/L, during CMDs (0.77 mWb/m· s) was between the transfer rates for two other modes (loading 0.62 mWb/m· s and unloading 0.80 mWb/m· s). All transfer rates had very low steadiness values; CV was 190% for loading, 160% for unloading and 180% for CMDs. However, since the rate of flux supply from dayside reconnection is greater for unloading and loading (ϕ_d = 3.0 mWb/m · s, on average) compared to continuous dissipation intervals (ϕ_d = 2.1 mWb/m · s, on average), the total rate of nightside reconnection ϕ_{Earth} needs to be greater for unloading as opposed to continuous dissipation. And since

ϕ_{Earth}/L is the same for both unloading and CMD intervals we may conclude that the length of the x-line in the tail, L, for unloading and loading modes is greater than L for continuous magnetospheric dissipation.

(3) Solar wind conditions leading to different convection modes were fairly variable. Only $IMF\ B_z$ showed clear tendency towards less negative values for CMD mode; typical $\mu(IMF\ B_{z,sw})$ for continuous dissipation mode was -4.8 nT and about -6.5 nT for loading and unloading modes. The steadiness of $IMF\ B_z$ did not seem to be a critical precursor for continuous magnetospheric dissipation.

(4) Extended CMD periods, lasting longer than 3 hours were observed when the magnetotail was driven smoothly with only slightly negative $IMF\ B_z$. Three extended loading and four extended continuous dissipation periods were found from our data set. Average $IMF\ B_z$ was around -5 nT for extended loading intervals and about -4 nT for extended CMDs.

Acknowledgments. We wish to thank Geotail team for the tail magnetic and plasma data; ACE team for the solar wind magnetic and plasma data; IMAGE, CANOPUS, and Kyoto data centers for the ground-based magnetic observations. Fruitful discussions with S.-I. Akasofu, and V. Sergeev, and valuable comments of referee are acknowledged. The work of ET was supported by National Research Council and Academy of Finland.

References

Akasofu, S.-I., Energy coupling between the solar wind and the magnetosphere, *Space Sci. Rev., 28*, 121, 1981

Aubry, M.P., A Short review of magnetospheric substorms, *Earth's magnetospheric processes*, Proceedings of a Symposium, org. by the Summer Advanced Study Institutem and 9th ESRO Summer School, Italy in 1971, Vol. 32, p.357, 1971

Angelopoulos, V., Baumjohann, W., Kennel, C.F., Coronti, F.V., Kivelson, M.G., Pellat, R., Walker, R.J., Luehr, H., Paschmann, G., Bursty bulk flows in the inner central plasma sheet, *J. Geophys. Res.,* , 97, A4, 4027, 1992

Angelopoulos, V., C.F. Kennel, F.V. Korotini, R. Pellat, H.E. Spence, M.G. Kivelson, R.J. Walker, W. Baumjohann, W.C. Feldman, J.T. Gosling, Characteristics of ion flow in the quiet state of the inner plasma sheet, *Geophys. Res. Lett.,* , 20, 16, 1711, 1993

Baumjohann, W., Paschmann, G., & Luehr, H., Characteristics of high-speed ion flows in the plasma sheet, *J. Geophys. Res.,* , 95, 3801, 1990

Borovsky, J.E., R.J. Nemzek, and D. Belian, The occurrence rate of magnetospheric substorm onsets; Random and periodic substorms, *J. Geophys. Res.,* , 98, A3, p. 3807, 1993

Caan, M.N., McPherron, R.L., and Russell, C.T., Solar wind and substorm related changes in the lobes of the geomagnetic tail, *J. Geophys. Res., 78*, 8087, 1973

Caan, M.N., McPherron, R.L., and Russell, C.T., The statistical magnetic signatures of magnetospheric substorm, *Planet. Space Sci., 26*, 269, 1978

Erickson G.M. and R.A. Wolf, Is steady convection possible in the Earth's magnetosphere?, *Geophys. Res. Lett., 7*, 897, 1980

Fairfield, D.H., R.P. Lepping, E.W. Hones, Jr., S.J. Bame, and J.R. Asbridge, Simultaneous measurements of magnetotail dynamics by IMP spacecraft, *J. Geophys. Res.,* , 86, A3, p. 1396, 1981

Fairfield and Cahill, Transition region magnetic field and polar magnetic disturbances, *J. Geophys. Res.,* , 71, 155, 1966

Huang, C., G.D., Reeves, J.E., Borovsky, R.M., Skoug, Z.Y., Pu, and G. Le, Periodic magnetospheric substorms and their relationship with solar wind variations, *Geophys. Res. Lett.,* , 108, NO A6, p. 1255, doi: 10.1029/2002JA009704, 2003

Kamide, Y., Two-component aurora electrojet, *Geophys. Res. Lett.,* , 9, p. 1175, 1982

Lee, L.C., Fu, Z. F., Akasofu, S.-I., A simulation study of forced reconnection processes and magnetospheric storms and substorms, *J. Geophys. Res.,* , 90, A11, 10 896, 1985

McPherron, R. L., C.T. Russell, and M.P. Aubry, Satellite studies of magnetospheric substorms on August 15, 1968: Phenomenological model for substorms *J. Geophys. Res.,* , 78, 3131, 1973

Nagai, T, Fujimoto, M., Nakamura, R., Saito, Y., Mukai, T., Yamamoto, T., Nishida, A., Kokobun, S., Reeves, G.D., Lepping, R.P., Geotail observations of a tailward flow at X_{GSM} = -15R_E, *J. Geophys. Res.,* , 103, A10, 23543, 1998

O'Brien, T. P., Thompson, S. M., & McPherron, R. L., Steady magnetospheric convection: Statistical signatures in the solar wind and AE, *Geophys. Res. Lett.,* , Vol 29, 7, p. 34, 2002

Pachmann, G.B., U.O. Sonnerup, I. Papamastorakis, N. Sckopke, G. Haerendel, S.J., Bame,

J.R., Asbridge, J.T. Gosling, C. T. Russell, and R.E., Elphic, Plasma acceleration at the Earth's magnetopause: Evidence for reconnection, *Nature, 282*, 243-246, 1979

Petrukovich, A.A., T., Mukai, S. Kokobun, S.A., Romanov, Y., Saito, T., Yamamoto, and L.M. Zelenyi, Substorm-associated pressure variations in the magnetotail plasma sheet and lobe, *J. Geophys. Res.,* , 104, A3, p. 4501, 1999

Pytte, T., McPherron, R. L., Hones, E. W., & West, H. I., Multiple-Satellite Studies of Magnetospheric Substorms: Distinction between Polar Magnetic Substorms and Convection Driven Negative Bays, *J. Geophys. Res.,* , 83, 663, 1978

Russell, C.T., and R.L., McPherron, The magnetotail and substorms, *Space Sci. Rev., 28*, 15, p. 205, 1973

Sergeev, V. A., Pellinen, R. J., & Pulkkinen, T. I., Steady magnetospheric convection: A Review of recent results, *Space Sci. Rev., 75*, 551, 1996A

Sergeev, V. A., Pulkkinen, T.I., & Pellinen, R.J., Coupled-mode scenario for the magnetospheric dynamics, *J. Geophys. Res.,* , Vol 101, A6, 13047, 1996B

Sergeev, V.A., Lennartsson, W., Pellinen, R.J., and Vallinkoski, M., Average patterns of precipitation and plasma flow in the plasma sheet flux tubes during steady magnetospheric convection, *Planetary Space Science*, 38, 231, 1999

Sergeev, V.A., P., Tanskanen, K. Mursula, A. Korth, R.C., Elphic, Current sheet thickness in the near-earth plasma sheet during substorm growth phase, *J. Geophys. Res.,* , 95, p. 3819, 1990

Sergeev, V.A., and Lennartsson, W., Plasma sheet at X -20 Re during steady magnetospheric convection, *Planet. Space Sci.*, 36, p. 353, 1988

Sergeev, On the state of the magnetosphere during prolonged periods of southward oriented IMF, Phys. Solariterr., Potsdam, 5, 39, 1977

Shukhtina, M.A., N. P. Dmitrieva, and V. A. Sergeev, Quantitative magnetotail characteristics of different magnetotail states, *Annales Geophysicae*, 22, p. 1019, 2004

Slavin, J.A., C.J. Owen, M.W., Dunlop, E. Borälv, M.B., Moldwin, D.G., Sibeck, E., Tanskanen, M.L., Goldstein, A., Fazakerley, A., Balogh, E., Lucek, I. Richter, H., Reme, and J.M. Bosqued, Cluster four spacecraft measurements of small traveling compression regions in the near-tail, *Geophys. Res. Lett.,* , doi:10.1029/2003GL018438, 2003

Slavin, J. A., Smith, M. F., Mazur, E. L., Baker, D. N., Iyemori, T., Singer, H. J., & Greenstadt, E. W., ISEE 3 plasmoid and TCR observations during an extended interval of substorm activity, *Geophys. Res. Lett.,* , 19, 825, 1992

Spence, H.E., Kivelson, M.G., and Walker, R.J., Static magnetic field models consistent with nearly isotropic plasma pressure, *Geophys. Res. Lett.,* , 14, 872, 1987

Tanskanen, E.I., T.I. Pulkkinen, H.E.J. Koskinen, and J.A. Slavin, Substorm energy budget near solar minimum and maximum: 1997 and 1999 compared, *J. Geophys. Res.,* , 107 (A6), 10.1029/2001JA900153, 2002

Yahnin, A., Malkov, M.V., Sergeev, V.A., Pellinen, R.J., Aulamo, O., Vennergstrom, S., Friis-Christensen, E., Lassen, K., Danielsen, C. and Crave, J.D., Features of steady magnetospheric convection, *J. Geophys. Res.,* , 99 (A3), 4039, 1994

Yermolaev, Yu.I., V.A. Sergeev, L.M. Zelenyi, A.A. Petrukovich, J.-A. Sauvaud, T., Mukai, S. Kokobun, Two spacecraft observation of plasma convection jet during continuous external driving, *Geophys. Res. Lett.,* , 26, NO2, p. 177, 1999

Received 2004; revised 200x

To appear in the *Journal of Geophysical Research*, 200x.

This manuscript was prepared with AGU's LaTeX macros v5, with the extension package 'AGU^{++}' by P. W. Daly, version 1.6b from 1999/08/19.

Appendix A: List of 52 events when the $IMF\ B_z$ is southward longer than 8 hours.

Table A1.

Intervals of time when the ACE interplanetary magnetic field is southward longer than 8 hours. Geotail tail seasons November through April, 1999 from 2002 are examined.

Figure Captions

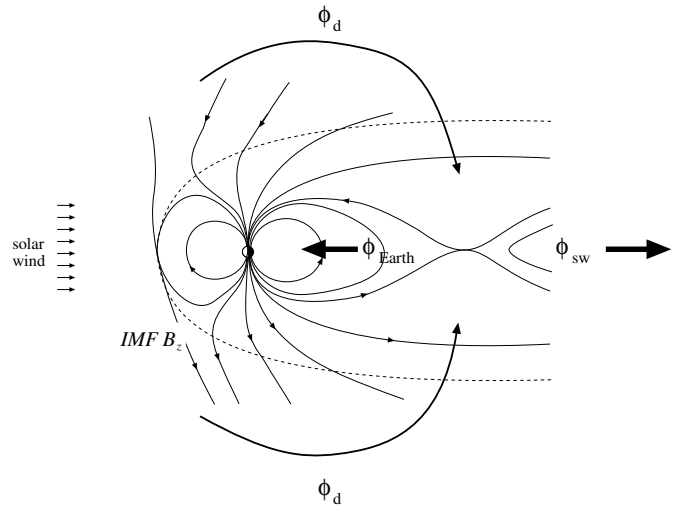

Figure 1. Cartoon of magnetospheric convection: dayside-to-nightside flux transfer rate (ϕ_d), nightside-to-dayside flux transfer rate (ϕ_{Earth}), and nightside-to-solar wind flux transfer rate (ϕ_{sw}). To produce a continuous magnetospheric dissipation (CMD), $\int \phi_d(t)\ dt$ and $\int \phi_{Earth}(t)\ dt$ over the mode interval needs to be equal.

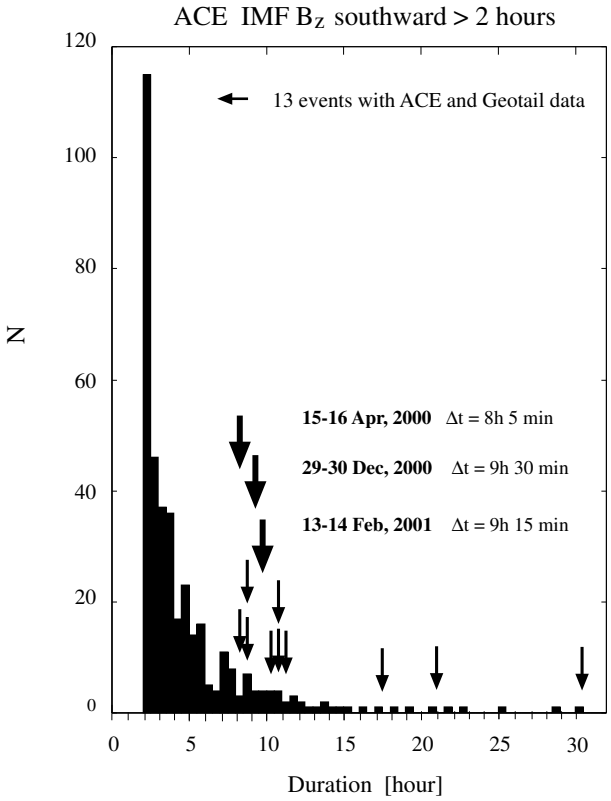

Figure 2. Histogram of the southward *IMF* B_z intervals longer than two hours identified during three latest Geotail tail seasons, November through April from 1999 to 2002. The black arrows mark the events lasting longer than 8 hours with both ACE and Geotail data when the Geotail was required to locate in the tail further than 10 R_E from the Earth.

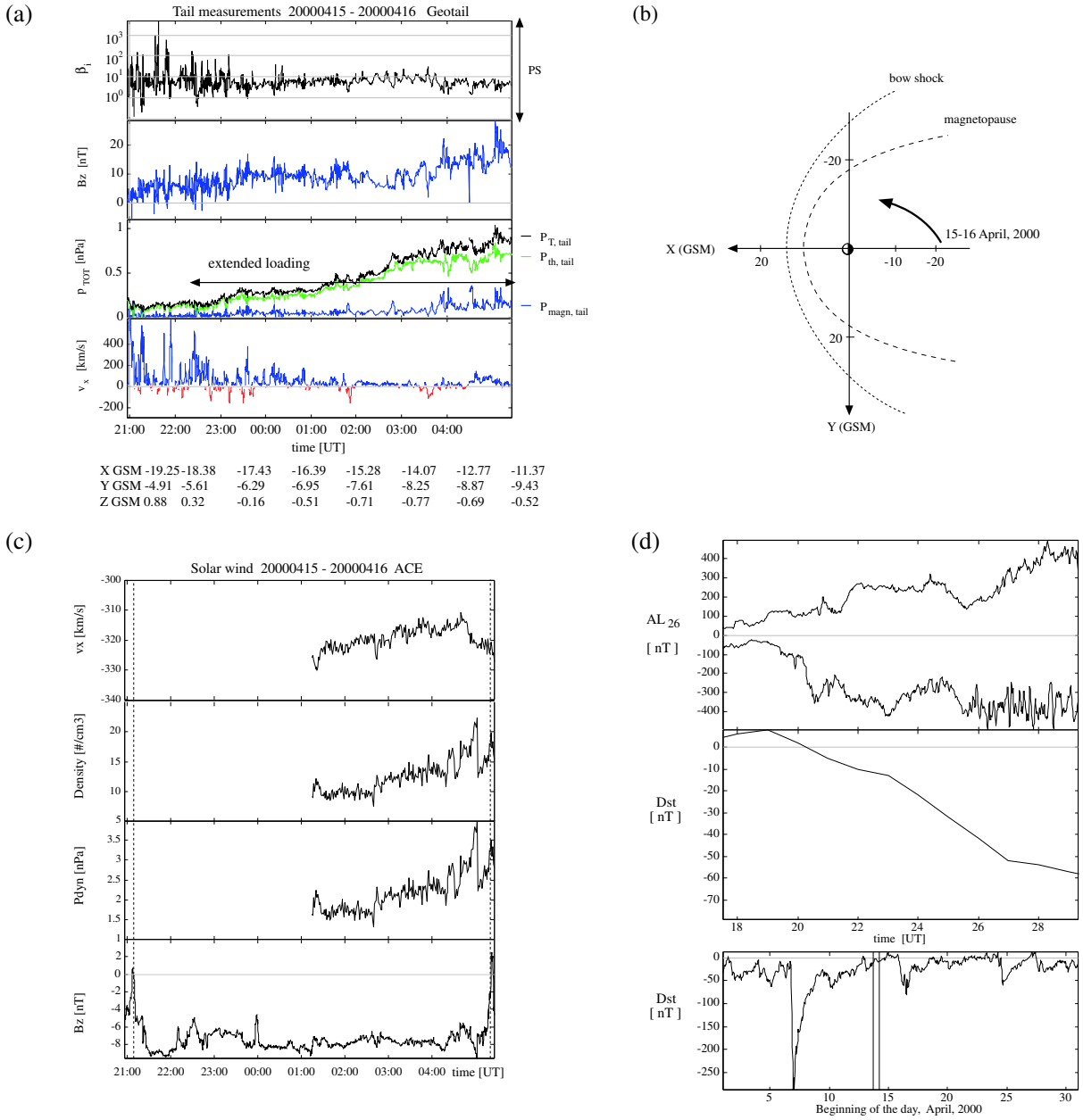

Figure 3. An example of an extended loading mode, April 15-16, 2000. (a) Tail measurements: plasma ion beta ($\beta_{i,tail}$), z-component of the magnetic field ($B_{z,tail}$), total pressure (p_{tot}), and x-component of the tail flow velocity ($v_{x,tail}$). (b) Geotail trajectory. (c) Solar wind measurements: x-component of velocity (v_x, sw), ion density (N_i), dynamic pressure ($p_{dyn,sw}$) and z-component of the interplanetary magnetic field (B_z). (d) Ground-based magnetic measurements: extended AL-index and dst index.

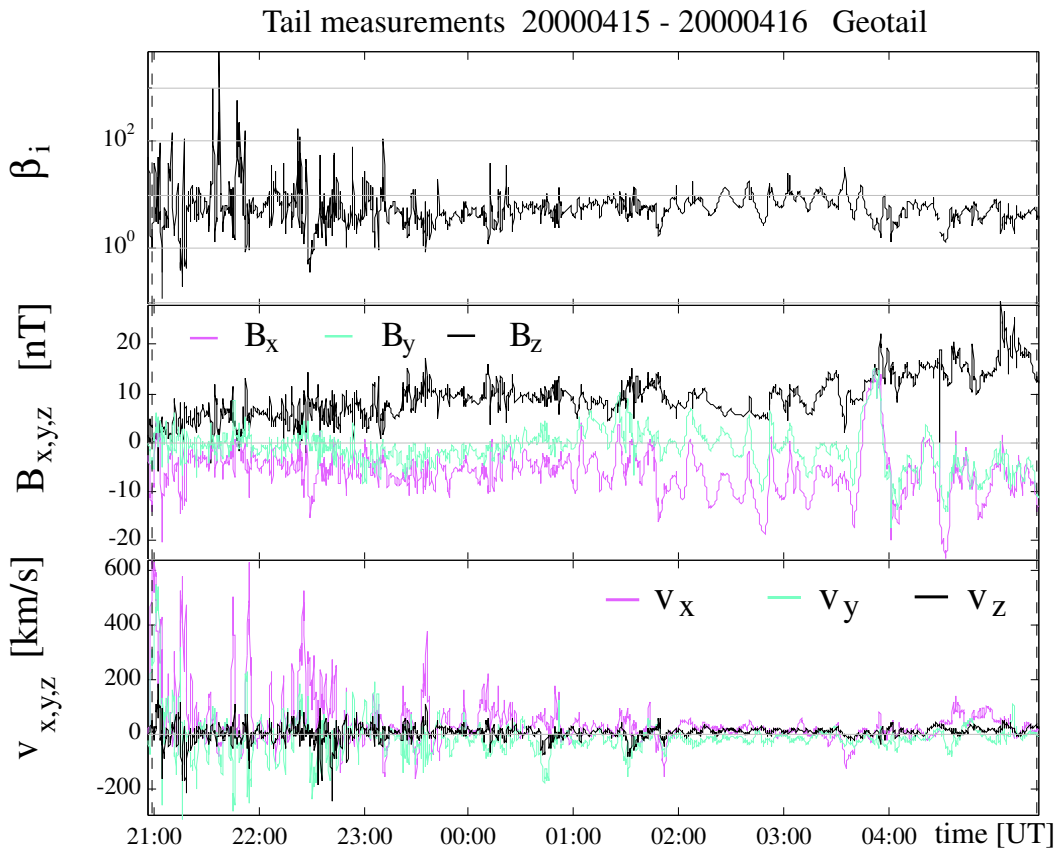

Figure 4. Components of tail magnetic field and plasma bulk velocity showing the slowness of the tail convection during extended loading period, April 15-16, 2000.

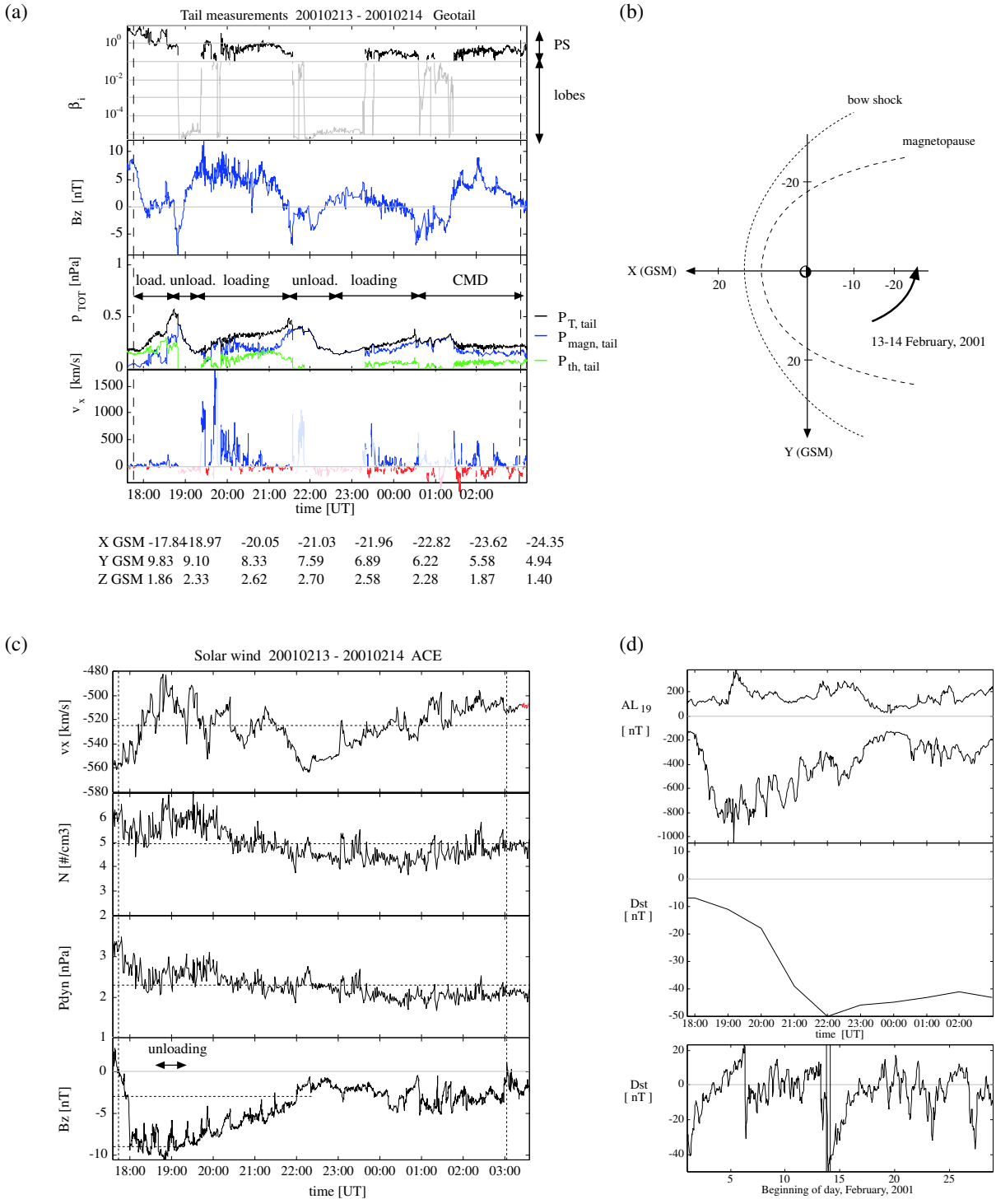

Figure 5. Two examples of an unloading mode, February 13-14, 2001. (a) Tail measurements in similar order as in Figure 3a. (b) Geotail trajectory. (c) Solar wind measurements in similar order as in Figure 3c. (d) Extended AL-index and dst-index.

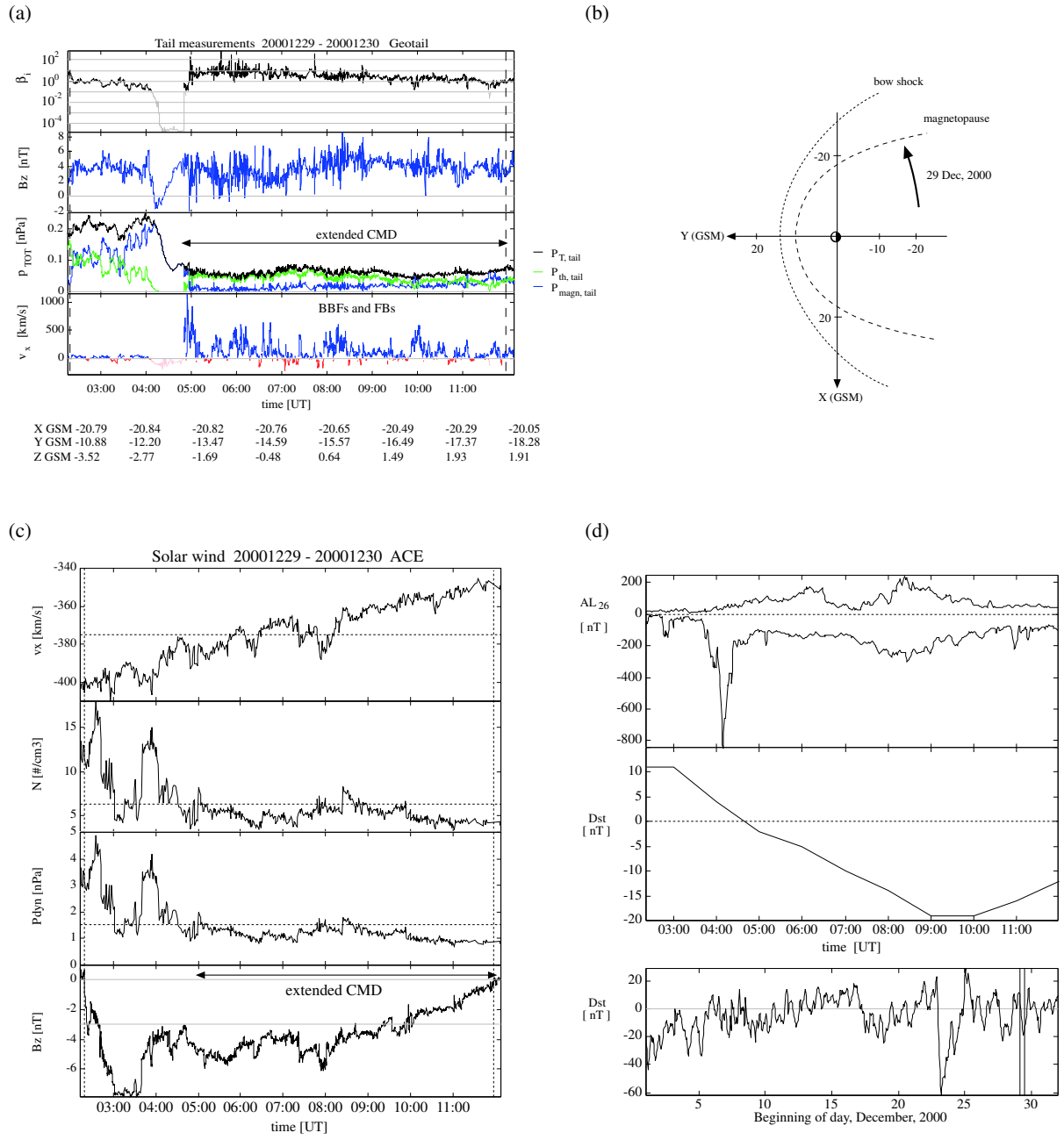

Figure 6. An example of a continuous magnetospheric dissipation, December 29, 2000. (a) Tail measurements in similar order as in Figure 3a. (b) Geotail trajectory. (c) Solar wind measurements in similar order as in Figure 3c. (d) Extended AL-index and dst-index.

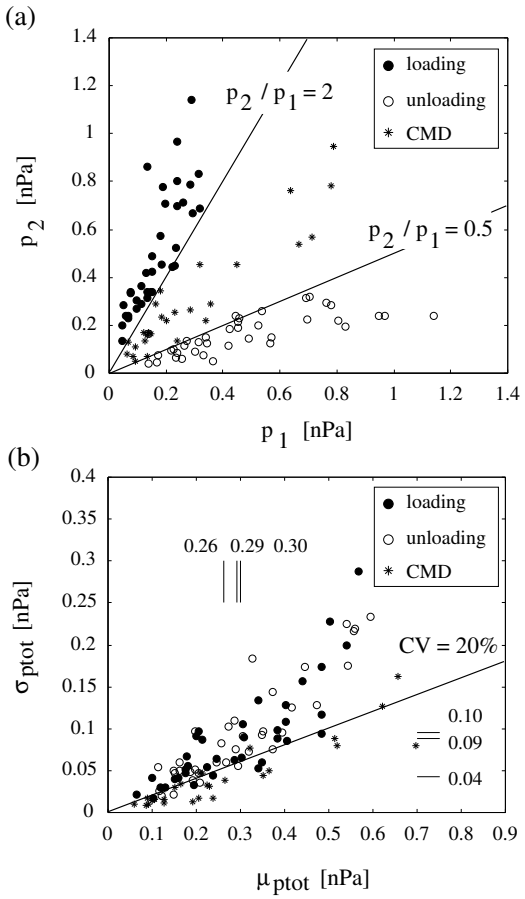

Figure 7. (a) Earth's magnetotail convection modes identified from tail total pressure: (1) loading, (2) unloading, and (3) continuous magnetospheric dissipation. Magnetotail total pressure in the beginning of the mode interval is marked by p_1 and total pressure in the end of the mode interval by p_2.(b) Average tail total pressure versus standard deviation for loading (black circle), unloading (white circles) and continuous dissipation (stars).

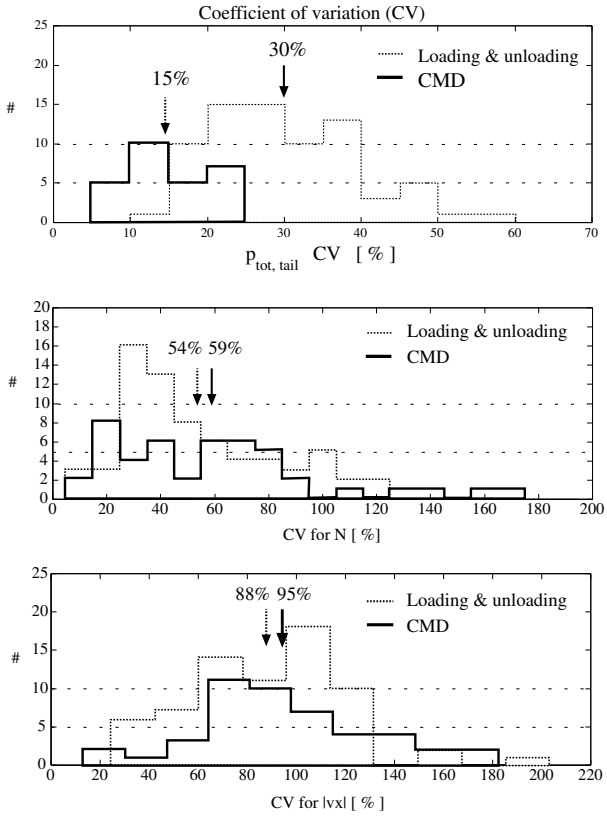

Figure 8. Histograms of the steadiness of tail total pressure separately for substorms (loading/unloading) and for continuous magnetospheric dissipation. Histograms are binned by every 10 %

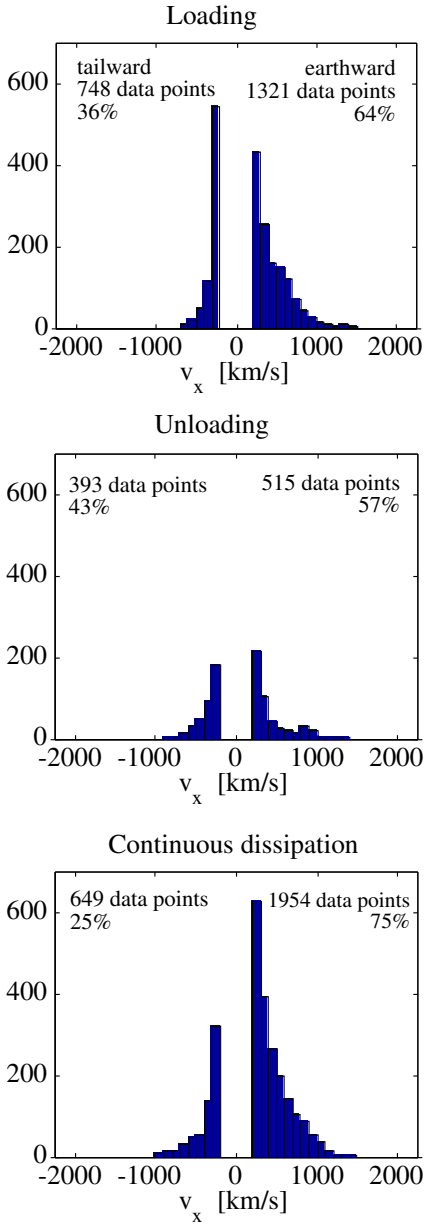

Figure 9. Histograms of the entire velocity data separately for three convection modes. Velocities smaller than 200 km/s are excluded.

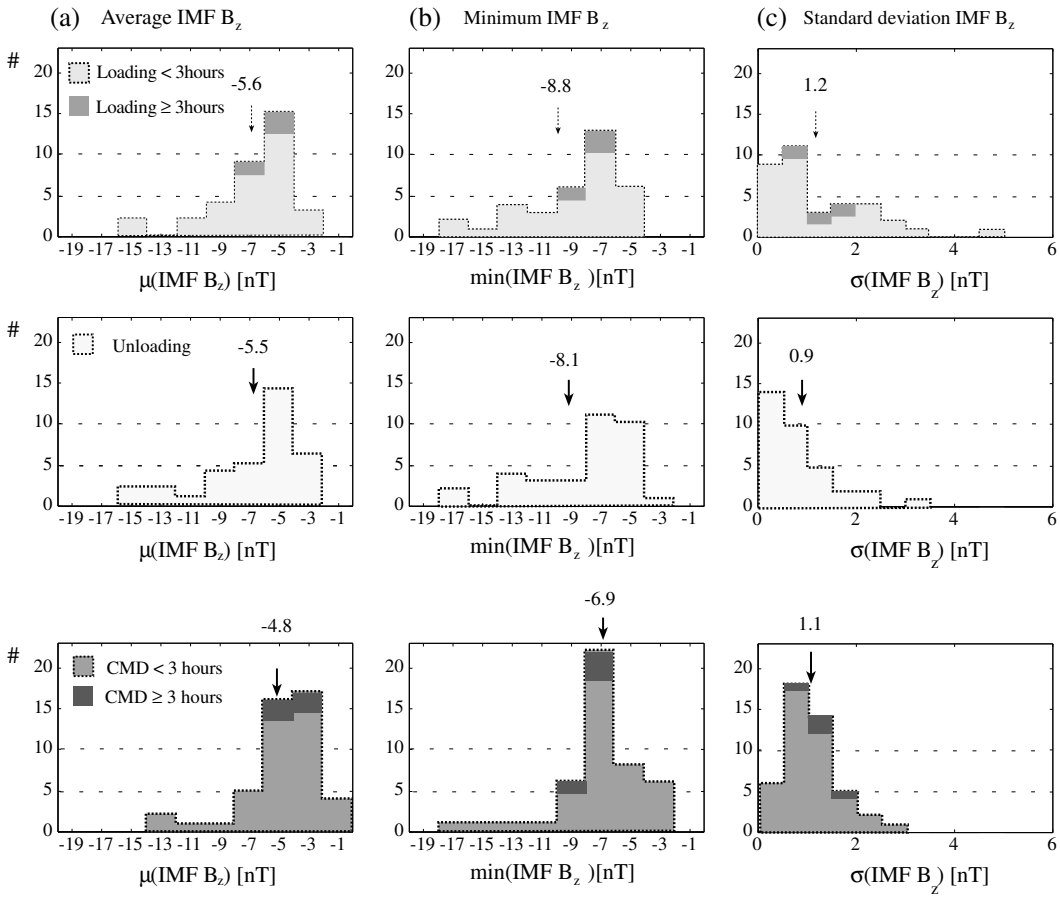

Figure 10. Histograms of (a) average southward $IMF\ B_{z,sw}$, (b) minimum southward $IMF\ B_{z,sw}$, and (c) standard deviation of $IMF\ B_{z,sw}$ separately for three convection modes. Extended intervals lasting more than 3 hours are marked by dark grey. Histograms in (a) and (b) are binned by every 2 nTs in (c) every 0.5 nTs.

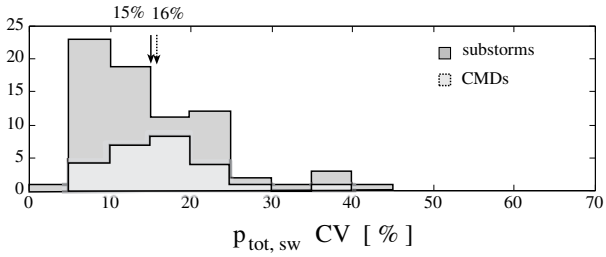

Figure 11. Histograms of solar wind total pressure separately for substorms (loading/unloading) and continuous magnetospheric dissipation.

Tables

Year	Month	Day	t_1			t_2			Duration	
			h	min	s	h	min	s	h	min
1999	11	12	18	23	12	39	15	12	21	52
1999	11	14	04	57	20	16	20	16	11	22
1999	11	16	07	40	32	15	57	36	8	17
1999	11	19	07	02	07	18	57	03	12	55
1999	11	23	05	50	39	17	36	47	12	46
1999	12	27	17	10	35	28	50	03	12	39
2000	01	17	21	49	45	29	59	38	8	10
2000	01	22	16	50	32	26	17	30	9	27
2000	01	23	22	56	10	32	42	33	10	46
2000	01	24	16	28	41	33	20	09	17	51
2000	02	17	11	40	38	22	03	50	10	23
2000	03	08	13	12	36	22	04	04	9	51
2000	03	10	09	50	44	26	39	47	17	49
2000	03	11	10	43	15	19	48	35	9	5
2000	03	30	12	25	52	20	52	32	8	26
2000	04	02	18	28	49	38	21	52	20	53
2000	04	04	17	42	25	25	45	53	8	3
2000	04	10	07	35	11	16	05	35	9	30

2000	04	15	18	37	51	28	07	26	9	29
2000	11	06	22	03	49	33	34	12	12	30
2000	11	28	20	58	58	32	09	22	11	10
2000	12	01	10	36	51	19	20	35	9	44
2000	12	04	17	39	14	39	21	06	22	42
2000	12	22	22	21	35	37	41	19	15	20
2000	12	29	01	11	58	10	50	22	10	38
2001	01	11	11	13	32	23	09	32	12	56
2001	01	21	06	02	52	19	56	60	14	54
2001	01	24	08	37	48	19	31	08	11	53
2001	01	26	01	42	03	17	20	59	16	39
2001	01	28	00	33	31	11	04	59	11	31
2001	02	13	16	56	09	26	15	04	9	20
2001	03	04	13	51	35	25	58	47	12	7
2001	03	12	17	14	29	25	00	05	8	46
2001	03	18	19	47	49	30	25	39	11	38
2001	04	01	19	02	43	32	48	35	14	46
2001	04	15	16	28	17	35	49	05	19	21
2001	04	18	17	38	25	36	33	04	19	55
2001	04	22	03	31	13	32	19	59	29	49
2001	04	28	19	46	55	29	44	46	10	58

2001	10	31	18	06	32	41	08	08	23	2
2001	11	05	19	31	04	29	02	31	10	31
2001	11	06	18	35	19	27	34	15	9	59
2001	11	10	18	51	35	27	49	43	9	58
2001	12	12	07	31	32	30	51	46	23	20
2001	01	04	18	20	32	27	35	44	9	15
2002	02	02	01	33	00	11	06	20	10	33
2002	02	28	18	56	56	27	06	33	8	10
2002	03	03	11	22	16	21	56	24	11	34
2002	03	23	17	37	41	26	17	58	9	40
2002	03	24	11	37	26	20	29	10	9	52
2002	04	17	23	40	18	49	43	30	26	3
2002	04	20	03	03	14	20	35	30	18	32